

Super-resolution in incoherent optical imaging using synthetic aperture with Fresnel elements

Barak Katz* and Joseph Rosen

*Department of Electrical and Computer Engineering
Ben Gurion University of the Negev, P.O Box 653, Beer-Sheva 84105, Israel
barakk@ee.bgu.ac.il

Abstract: We present a new lensless incoherent holographic system operating in a synthetic aperture mode. Spatial resolution exceeding the Rayleigh limit of the system is obtained by tiling digitally several Fresnel holographic elements into a complete Fresnel hologram of the observed object. Each element is acquired by the limited-aperture system from different point of view. This method is demonstrated experimentally by combining three holographic elements recorded with white light illumination which is emitted from a binary grating.

©2010 Optical Society of America

OCIS codes: (090.0090) Holography; (280.6730) Synthetic aperture radar; (100.6890) Three-dimensional image processing; (170.6900) Three-dimensional microscopy.

References and links

1. S. M. Beck, J. R. Buck, W. F. Buell, R. P. Dickinson, D. A. Kozlowski, N. J. Marechal, and T. J. Wright, "Synthetic-aperture imaging laser radar: laboratory demonstration and signal processing," *Appl. Opt.* **44**(35), 7621–7629 (2005).
2. V. Mico, Z. Zalevsky, P. García-Martínez, and J. García, "Synthetic aperture superresolution with multiple off-axis holograms," *J. Opt. Soc. Am. A* **23**(12), 3162–3170 (2006).
3. L. Martínez-León, and B. Javidi, "Synthetic aperture single-exposure on-axis digital holography," *Opt. Express* **16**(1), 161–169 (2008).
4. G. Indebetouw, Y. Tada, J. Rosen, and G. Brooker, "Scanning holographic microscopy with resolution exceeding the Rayleigh limit of the objective by superposition of off-axis holograms," *Appl. Opt.* **46**(6), 993–1000 (2007).
5. J. Rosen, and G. Brooker, "Digital spatially incoherent Fresnel holography," *Opt. Lett.* **32**(8), 912–914 (2007).
6. J. Rosen, and G. Brooker, "Fluorescence incoherent color holography," *Opt. Express* **15**(5), 2244–2250 (2007).
7. J. Rosen, and G. Brooker, "Non-Scanning Motionless Fluorescence Three-Dimensional Holographic Microscopy," *Nat. Photonics* **2**(3), 190–195 (2008).
8. J. W. Goodman, *Introduction to Fourier Optics*, 2nd ed. (McGraw-Hill, New York, 1996), pp. 314–317.

1. Introduction

Synthetic aperture is a well-known super-resolution technique which extends the resolution capabilities of an imaging system beyond the theoretical Rayleigh limit dictated by the system's actual aperture. Using this technique, several patterns acquired by an aperture-limited system, from various locations, are tiled together into one large pattern which could be captured only by a virtual system equipped with a much wider synthetic aperture.

The utilization of optical holography for synthetic aperture is usually restricted to coherent imaging [1–3]. Therefore, the use of this technique is limited only to those applications in which the observed targets can be illuminated by a laser. Synthetic aperture carried out by a combination of several off-axis incoherent holograms in scanning holographic microscopy has been demonstrated by Indebetouw et al [4]. However, this method is limited to microscopy only, and although it is a technique of recording incoherent holograms, a specimen should also be illuminated by an interference pattern between two laser beams.

The holographic method proposed in this study is based on the recently invented system of a single-channel incoherent interferometer employed for generating digital Fresnel holograms [5–7]. In this non-scanning holographic technique, incoherent light is reflected or emitted from a three dimensional (3-D) object, then propagates through a spatial light modulator (SLM), and is finally recorded by a digital camera. The SLM is used as a diffractive beam

splitter of the incoherent interferometer, so that each spherical beam, originated from each object point, is split into two spherical beams with two different curve radii. Accumulation of the entire interferences within all of the couples of spherical beams creates the Fresnel hologram of the observed object. Three holograms are recorded sequentially, each for a different phase factor of the SLM. The three holograms are superposed in the computer, so that the result is a complex-valued Fresnel hologram that does not contain the twin image and the bias term. It should be noted that the term incoherent light in this study means quasi-monochromatic spatially incoherent light. The property of quasi-monochromatic light is achieved by placing a chromatic band-pass filter (BPF) at the system input.

In this paper we propose a new scheme, dubbed a synthetic aperture with Fresnel elements (SAFE), for holographic imaging of incoherently illuminated objects. The proposed lensless system contains a BPF, a polarizer, an SLM and a digital camera. This holographic system has an extended synthetic aperture in order to improve the transverse and axial resolutions beyond the classic limitations. The term synthetic aperture, in the present context, means time (or space) multiplexing of several Fresnel holographic elements captured from various viewpoints by a system with a limited real aperture. The synthetic aperture is implemented by shifting the BPF-polarizer-SLM-camera set, located across the field of view, among several viewpoints. At each viewpoint a different mask is displayed on the SLM, and a single element of the Fresnel hologram is recorded (See Fig. 1). The various elements, each of which is recorded by the real aperture system during the capturing time, are tiled together so that the final mosaic hologram is effectively considered as captured from a single synthetic aperture which is much wider than the actual aperture.

2. Analysis of SAFE

An example of a system with the synthetic aperture, which is three times wider than the actual aperture, can be seen in Fig. 1. To simplify the demonstration, the synthetic aperture was implemented only along the horizontal axis. In principle this concept can be generalized for both axes and for any ratio of synthetic to actual apertures. Imaging with the synthetic aperture is necessary for cases where the angular spectrum of the light emitted from the observed object is wider than the numerical aperture of a given imaging system. In SAFE shown in Fig. 1, the SLM and the digital camera move in front of the object. The complete Fresnel hologram of the object, located at some distance from the SLM, is a mosaic of 3 holographic elements, each of which is recorded from a different point of view by the system with the real aperture which is $A_x \times A_y$ in size. In this specific example, the complete hologram tiled from the 3 holographic Fresnel elements has the synthetic aperture which is $3 \cdot A_x \times A_y$ in size, and it is 3 times larger than the real aperture at the horizontal axis. An object point located at the point (x_s, y_s, z_s) , at a distance z_s from the SLM, induces a tilted diverging spherical wave of the form of $C_1(\bar{r}_s)Q[1/z_s]L[-\bar{r}_s/z_s]$ on the SLM plane (x, y) , where for the sake of simplification, the quadratic phase function is designated by the function Q , such that $Q[s] = \exp[i\pi s \lambda^{-1}(x^2 + y^2)]$, and the linear phase function is designated by the function L , such that $L[\bar{s}] = \exp[i2\pi \lambda^{-1}(s_x x + s_y y)]$. λ is the average wavelength, $\bar{r}_s \equiv (x_s, y_s)$ and $C_1(\bar{r}_s)$ is a complex constant dependent on the source point's location.

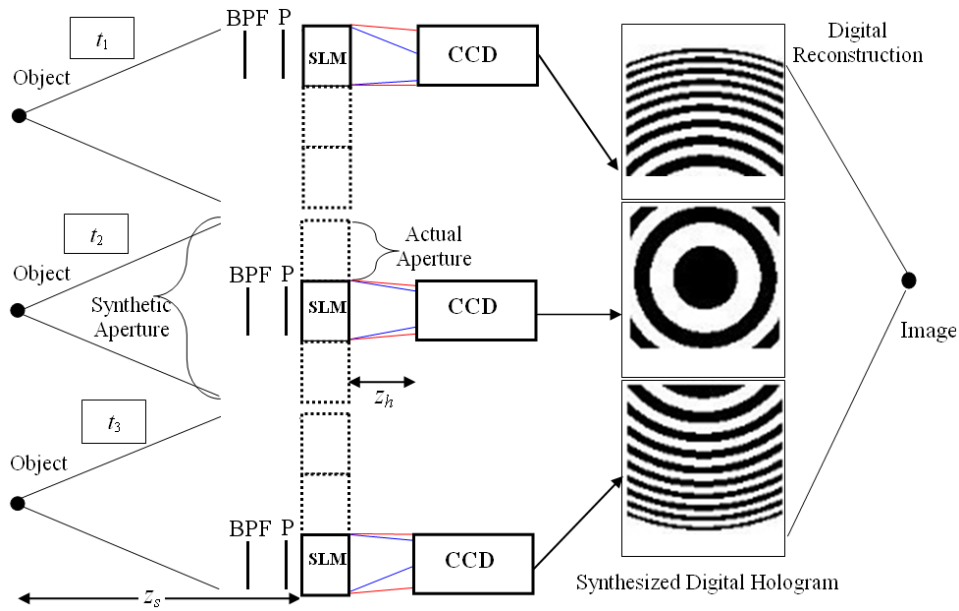


Fig. 1. Scheme of SAFE operating as synthetic aperture radar to achieve super-resolution. P indicates polarizer.

Each tilted diverging spherical wave in the (m, n) -th exposure is split into two waves by the SLM mask which is a sum of two aperture-limited quadratic phase functions of the form, $(C_2Q[-1/f_1] + C_3Q[-1/f_2])\text{rect}\left[\frac{x - A_x \cdot m}{A_x}, \frac{y - A_y \cdot n}{A_y}\right]$, where f_1, f_2 are real constants indicating the focal distances of the two diffractive lenses, $C_{2,3}$ are complex constants and

$$\text{rect}\left(\frac{x}{\alpha}, \frac{y}{\beta}\right) \equiv \begin{cases} 1 & (|x|, |y|) \leq (\alpha/2, \beta/2) \\ 0 & \text{Otherwise} \end{cases}$$

From the SLM plane the two waves propagate a distance z_h till they are recorded by the digital camera. The complex amplitude on the camera plane (x_o, y_o) is computed as a free-space propagation under Fresnel approximation or, in other words, as a convolution between the complex amplitude on the SLM and the function $Q[1/z_h]$. A complete Fresnel hologram of the object point located at (x_s, y_s, z_s) is a sum of $M \times N$ holographic elements, each of which is the intensity recorded from the (m, n) -th location by the digital camera as the following:

$$I_h(x_o, y_o; x_s, y_s, z_s) = \sum_{n=\frac{1-N}{2}}^{\frac{N-1}{2}} \sum_{m=\frac{1-M}{2}}^{\frac{M-1}{2}} \left| C_1(\bar{r}_s) Q\left[\frac{1}{z_s}\right] L\left[\frac{-\bar{r}_s}{z_s}\right] \cdot \left(C_2 Q\left[\frac{-1}{f_1}\right] + C_3 Q\left[\frac{-1}{f_2}\right] \right) \right. \\ \left. \times \text{rect}\left(\frac{x - A_x \cdot m}{A_x}, \frac{y - A_y \cdot n}{A_y}\right) * Q\left[\frac{1}{z_h}\right] \right|^2, \quad (1)$$

where the asterisk denotes a two dimensional convolution, and without the loss of generality, we assume that M and N are odd numbers. Following straightforward calculations detailed in the appendix, the intensity distribution recorded by the digital camera is expressed as the following:

$$I_h(x_o, y_o; x_s, y_s, z_s) = \left(C_4 + C_5(\bar{r}_s) Q \left[\frac{-1}{z_r} \right] \cdot L \left[\frac{-\bar{r}_r}{z_r} \right] + C_5^*(\bar{r}_s) Q \left[\frac{1}{z_r} \right] \cdot L \left[\frac{\bar{r}_r}{z_r} \right] \right) \times \sum_{n=\frac{1-N}{2}}^{\frac{N-1}{2}} \sum_{m=\frac{1-M}{2}}^{\frac{M-1}{2}} \text{rect} \left(\frac{x_o - A_x \cdot m}{A_x}, \frac{y_o - A_y \cdot n}{A_y} \right), \quad (2)$$

where

$$z_r = \frac{(f_1 z_s - z_h z_s + f_1 z_h)(f_2 z_s - z_h z_s + f_2 z_h)}{z_s^2 (f_1 - f_2)} \underset{f_2 \rightarrow \infty}{=} - \frac{(z_s + z_h)(f_1 z_s - z_h z_s + f_1 z_h)}{z_s^2}$$

$$\bar{r}_r = (x_r, y_r) = \frac{\bar{r}_s z_h}{z_s}$$

and $C_{4,5}$ are complex constants. z_r is the reconstruction distance of the point image from an equivalent optical hologram, although in the present case the hologram is of course digital, and the reconstruction is done by the computer. Note that z_r is obtained specifically in the case that one of the phase masks on the SLM is constant ($f_2 \rightarrow \infty$). This choice is used in the present experiment because practically the fill factor of the SLM is less than 100%, and therefore the constant phase modulation inherently exists in the SLM. Consequently, choosing $f_2 < \infty$ could cause unwanted three, instead of two, waves mixing on the hologram plane, one wave due to the constant phase and another two from the two different diffractive lenses.

Equation (2) is the expression of the transparency function of a hologram created by an object point and recorded by a conventional lensless Fresnel incoherent correlation holography (FINCH) [5–7] with a synthetic aperture which is $M \cdot A_x \times N \cdot A_y$ in size. This hologram has several unique properties. The transverse magnification M_T is expressed as $M_T = \partial x_r / \partial x_s = z_h / z_s$ (In contrast to a conventional Fresnel hologram [8], where $M_T = z_r / z_s$, and only in the latter expression z_s represents the distance between the object and the recording medium). The axial magnification is $M_A = \partial z_r / \partial z_s = z_h (2f_1 z_s + 2f_1 z_h - z_h z_s) / z_s^3$ (In contrast to a conventional hologram [8], where $M_A = M_T^2$). Based on these properties, and assuming the system is diffraction limited, the resolution limitations of the FINCH as an imaging system is that the minimum resolved object size is given by:

$$\Delta_{\min} = \max \left\{ \lambda / NA_{in}, \lambda / (M_T NA_{out}) \right\} = \max \left\{ 2\lambda z_s / D_{SLM}, 2\lambda z_r / (M_T D_{CCD}) \right\}, \quad (3)$$

where D_{SLM}, D_{CCD} are the diameters of the SLM, and the digital camera, respectively. NA_{in} and NA_{out} are the numerical aperture at the input and output of the complete holographic system, respectively. This result is in contrast to the resolution limit of a conventional Fresnel hologram in which the transverse magnification is $M_T = NA_{in} / NA_{out}$, and therefore the minimum resolved object size in case of the Fresnel coherent hologram is $\Delta_{\min} = 2\lambda z_s / D_H = 2\lambda z_r / M_T D_H$, where D_H is the diameter of a hologram. In other words,

in FINCH the resolution limitation can be dictated by either the input or the output apertures. In any event, however, the synthetic aperture system is an extension of both apertures. Substituting the various parameters in Eq. (3) indicates that for $D_{SLM} = D_{CCD} = D$ and for $f_1 < 0$, the resolution is always determined by the output aperture as proved by the following inequality:

$$\left| \frac{2\lambda z_s}{D_{SLM}} \right| = \left| \frac{2\lambda z_s}{D} \right| < \left| \frac{2\lambda z_r}{M_T D_{CCD}} \right| = \left| \frac{2\lambda z_r z_s}{z_h D} \right| = \left| \frac{2\lambda}{D} \cdot \frac{(z_s + z_h)(f_1 z_s - z_h z_s + f_1 z_h)}{z_h z_s} \right|$$

Using negative diffractive lens with $f_1 < 0$ is preferred in the lensless FINCH setup because the diverging lens guarantees a high visibility of the holographic interference fringes on the camera plane for any z_h distance.

Because the sum of the all of the *rect* functions in Eq. (2) becomes one *rect* function of the form $rect[x/(M \cdot A_x), y/(N \cdot A_y)]$, it is evident from Eq. (2) that the complete hologram tiled from $M \times N$ elements is a Fresnel hologram of a point with a synthetic aperture which is $M \cdot A_x \times N \cdot A_y$ in size, and it is $M \times N$ times larger than the real aperture. Therefore, for $N = M$, $f_1 < 0$ and $f_2 \rightarrow \infty$ the transverse resolution power of SAFE is higher than that of the real-aperture system by a number which is the inverse ratio between the minimal resolved sizes in these two cases as given by:

$$\frac{\Delta_{\min}^{RA}}{\Delta_{\min}^{SA}} = \frac{2\lambda z_r^{RA} / M_T D_{CCD}^{RA}}{2\lambda z_r^{SA} / M_T D_{CCD}^{SA}} = \frac{N(|f_1|z_s + z_h z_s + |f_1|z_h)}{N|f_1|z_s + z_h z_s + N|f_1|z_h} \quad (4)$$

where the superscript *RA* and *SA* stand for real and synthetic aperture, respectively. It is assumed in Eq. (4) that due to the finite size of the SLM pixels, increasing the SLM aperture (even synthetically) by N times compels us to increase the focal distance $|f_1|$ by the same rate. Equation (4) indicates that using synthetic aperture always improves the resolution performance of lensless FINCH, but the improvement is less than the ratio between the synthetic and the real apertures.

Equation (2) describes the Fresnel hologram obtained from a single object point, and therefore $I_h(x_o, y_o; x_s, y_s, z_s)$ is the point spread function (PSF) of the recording system in the synthetic aperture mode. The complete Fresnel hologram of a general incoherently-illuminated object $I_s(x_s, y_s, z_s)$ is an integral of the entire PSFs given by Eq. (2) over all object intensity distribution and is defined by:

$$H(x_o, y_o) = \iiint I_s(x_s, y_s, z_s) I_h(x_o, y_o; x_s, y_s, z_s) dx_s, dy_s, dz_s \quad (5)$$

Since the overall PSF given in Eq. (2) is identical to the PSF of the previous works [5–7], the mosaic hologram given in Eq. (5) is a Fresnel incoherent hologram of the object but with the property that this hologram has been recorded with the effective aperture which is $M \cdot A_x \times N \cdot A_y$ in size.

The method to eliminate the twin image and the bias term [two terms out of the three presented in Eq. (2)] is the same as has been used before [5–7]; three elemental holograms of the same object and for each point of view are recorded, each of the holograms has a different phase constant of the SLM's phase mask. The final holographic element is a specific superposition of the three recorded elements. The digital reconstruction of the final complex-valued mosaic hologram is conventionally computed by Fresnel back propagation.

3. Experimental Results

SAFE has been tested in the lab by the system shown in Fig. 1. Two types of objects have been tested. The first object is a binary grating with cycle length of 4 lines per *mm*, and the

second object is a combination of two binary gratings with different cycle length, one with 2 lines per *mm* and the other with 4 lines per *mm*. The distance from the object to the SLM has been 52 *cm*, and the distance between the phase-only SLM (Holoeye, PLUTO) and the digital camera (E-VISION, EVC6600SAM-GE5) has been 38.5 *cm*. A 100W Halogen ARC lamp has been used for objects illumination, and a BPF (with an 80 nm bandwidth surrounding 550 nm central wavelength) has been placed just in front of the SLM. The results of the experiments are summarized in Fig. 2 and in Fig. 3. In the first experiment we have recorded a hologram only by the actual aperture without shifting the system, in the setup shown in Fig. 1 at the time t_2 . Figure 2(a) shows one of the three masks displayed on the SLM in this experiment. Each of the three masks has one of the three different phase factors: 0° , 120° or 240° . As mentioned above, these three phase masks with different phase constants are required in order to eliminate the bias term and the twin image from the holographic reconstruction. As stated earlier, another problem with the SLM is that its fill factor is 87%, which means that part of the light is reflected from the SLM without any modulation. In order to avoid the interference of three waves projected on the camera, we have chosen one of the phase elements to be constant. The other phase element has been chosen to be a negative diffractive lens with the shortest focal distance that can be achieved with the SLM having the pixel size of 8 μm . The shortest focal distance guarantees maximum resolution power for a given aperture size. In the case of the actual aperture (1500×1000 pixels) and the synthetic aperture (3000×1000 pixels), the focal distances have been -34 *cm* and -68 *cm*, respectively. The NA_{in} is 0.0115 and 0.0231 for the *RA* and *SA*, respectively. The NA_{out} is 0.0035 and 0.0044 for the *RA* and *SA*, respectively. Note that the sum of two pure phase functions, i.e., the quadratic phase function $Q[-1/f_1]$ and the constant phase function, is no longer a pure phase function, but a complex function with non-constant magnitude. Since the SLM is a phase-only modulator, we use the previous method [5–7] of recording general complex function on a phase-only SLM. Each phase function is distributed randomly among half of the SLM pixels.

The three recorded holograms are superposed according to the same superposition equation given in Ref [5]. Figures 2(e), 2(g) and 3(a), 3(c) are the magnitude and the phase of the superposed holograms for the first and second object, respectively. It can be seen that the resolution along the horizontal direction of the reconstructed image, computed by Fresnel back propagation, is damaged in the sense that the image is lacking the original high-frequency gratings along the horizontal direction because the aperture is too narrow to capture the entire gratings spectral content. This damaged reconstructed image is shown in Fig. 2(i) (Media 1) for the first object and in Fig. 3(k) (Media 3) for the second object.

In the SAFE experiment nine different phase masks have been displayed on the SLM, three for each location of the SLM-camera set; left, central and right. Each of the masks has an actual aperture of 1500×1000 pixels. Each of the three masks at every location has one of the three different phase factors: 0° , 120° or 240° . In order to avoid edge effects on the recorded holograms there is an overlap of 750 pixels among the three actual apertures combining the synthetic aperture.

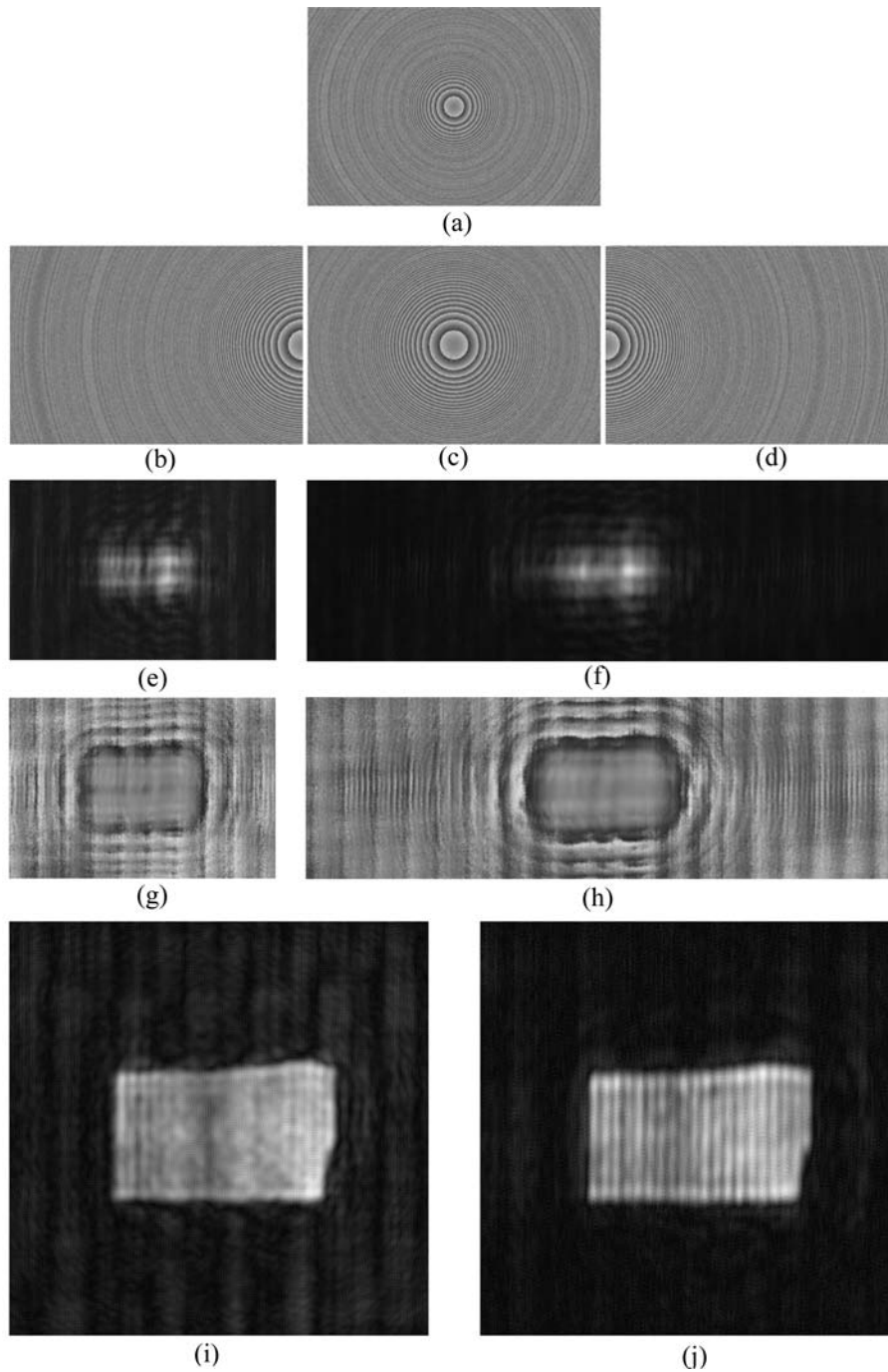


Fig. 2. Results of SAFE for the first object with the RA, and with the SA. (a) is the phase distribution of the reflection masks displayed on the SLM at $\theta = 120^\circ$ with the RA; (b)-(d) are the same as (a) using the SA; (e) is the magnitude of the final on-axis digital hologram with the RA, and (f) is the same as (e) with the SA; (g) is the phase of the final hologram with the actual aperture, and (h) is the phase with the synthetic aperture; (i) is the reconstruction of the binary grating at the best focus distance for the RA and (j) is for the SA. Movies of the holographic reconstructions that correspond to Fig. 2(i) and Fig. 2(j), respectively, can be viewed by pressing the cursor on [Media 1](#) and [Media 2](#).

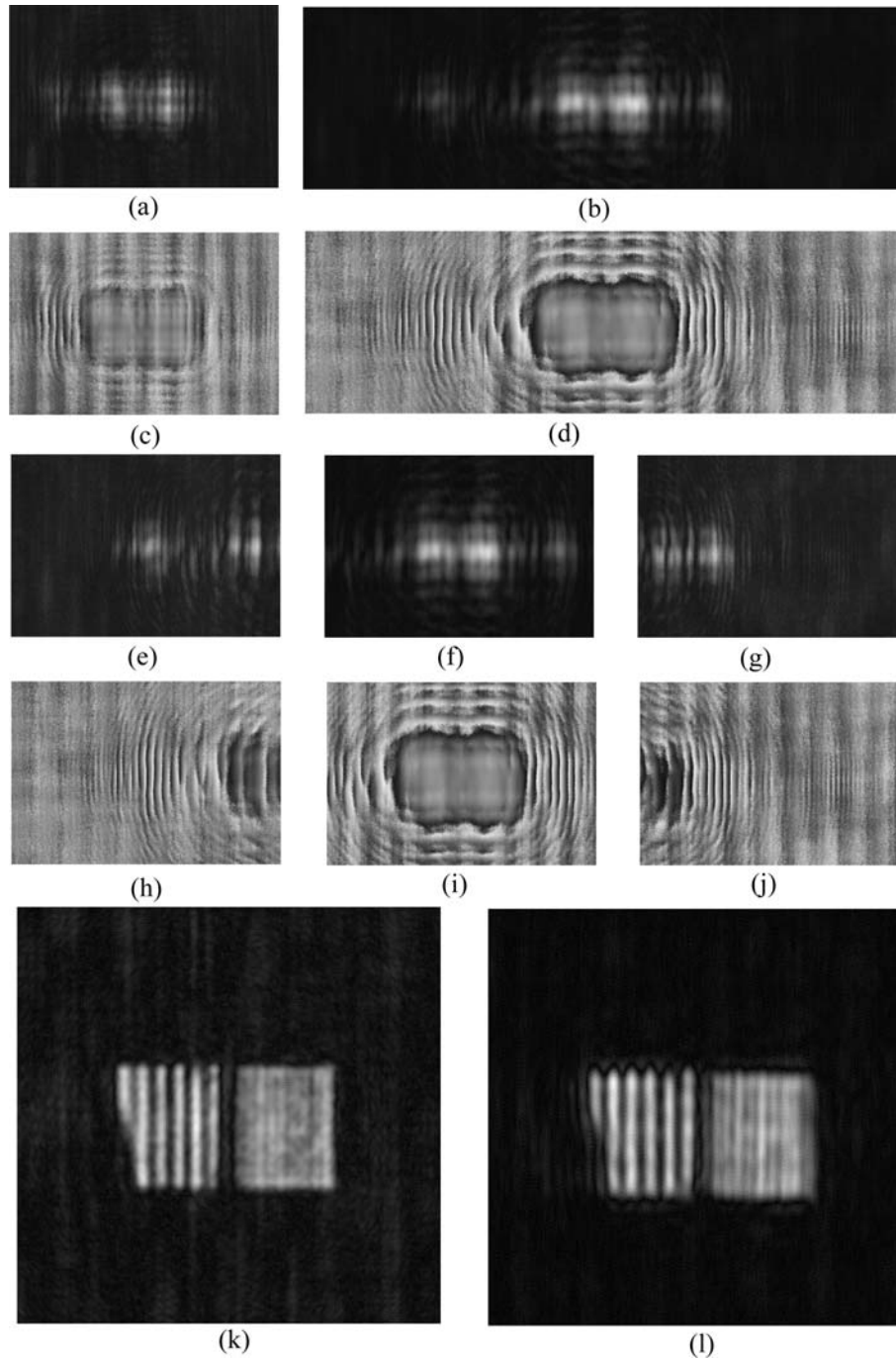


Fig. 3. Results of SAFE for the second object with the RA and with the SA. (a) and (c) are, respectively, the magnitude and the phase of the final on-axis digital hologram with the RA; (b) and (d) are, respectively, the magnitude and the phase of the final on-axis digital hologram with the SA; (e) is assembled from the magnitudes of the three holographic elements shown in (e)-(g), and (d) is assembled from the phases of three holographic elements shown in (h)-(j); (k) is the reconstruction of the hologram of the binary grating at the best focus distance for the RA, and (l) is for the SA. Movies of the holographic reconstructions that correspond to Fig. 3(k) and Fig. 3(l), respectively, can be viewed by pressing the cursor on [Media 3](#) and [Media 4](#).

For each location of the system, the three recorded holograms have been superposed as mentioned above. Figures 2(b)-2(d) represent three masks out of nine, each of which has been displayed at different time and at a different location of the setup along the horizontal axis. The superposed complex-valued holographic element from each system's viewpoint is stored in the computer. Upon completing the system movement along the entire synthetic aperture, all three holographic elements are tiled to a single mosaic hologram. Figures 2(f), 2(h) and 3(b), 3(d) represent the magnitude and the phase of the complete mosaic hologram for the first and for the second objects, respectively. Figures 3(e-g) and 3(h-j) are, respectively, the magnitude and the phase of the holographic elements from which the synthetic aperture mosaic hologram of the second object is assembled. The reconstruction result of the mosaic hologram, computed by Fresnel back propagation, is depicted in Fig. 2(j) (Media 2) for the first object, and Fig. 3(l) (Media 4) for the second object. The binary grating on the observed objects is seen well in the reconstructed images, indicating that the synthetic aperture is wide enough to acquire most of the horizontal spectral information of the objects. The movies, media 1 and media 2, emphasize the fact that the reconstruction planes presented in Figs. 2(i) and 2(j), are indeed the best focused planes of each reconstruction sequence, respectively, and the only parameter that influences better reconstruction quality of Fig. 2(j) compared to Fig. 2(i) is indeed the improved numerical aperture thanks to a successful synthetic aperture implementation. The same conclusion can be drawn comparing Figs. 3(k) and 3(l) shown in the movies, media 3 and media 4, respectively.

4. Conclusions

In this article, we have proposed and demonstrated a process of recording incoherent holograms in the synthetic aperture mode. The synthetic aperture of SAFE considerably increases both the transverse and the axial resolving power. To the best of our knowledge, this experiment is the first demonstration of a synthetic aperture radar in the visible light where the observed scene is illuminated by white light. The concept of the present system can be applied to all of the practices of imaging from microscopes to telescopes, as well as for both 2-D and 3-D imaging.

Appendix

In this appendix, we explain the process of deriving Eq. (2) from Eq. (1). Equation (1) is as the following:

$$I_h(x_o, y_o; x_s, y_s, z_s) = \sum_{n=\frac{1-N}{2}}^{\frac{N-1}{2}} \sum_{m=\frac{1-M}{2}}^{\frac{M-1}{2}} \left| C_1(\bar{r}_s) Q\left[\frac{1}{z_s}\right] L\left[\frac{-\bar{r}_s}{z_s}\right] \cdot \left(C_2 Q\left[\frac{-1}{f_1}\right] + C_3 Q\left[\frac{-1}{f_2}\right] \right) \right| \times \text{rect}\left(\frac{x - A_x \cdot m}{A_x}, \frac{y - A_y \cdot n}{A_y}\right) * Q\left[\frac{1}{z_h}\right] \Big|^2. \quad (6)$$

Next we calculate all the products of the Q functions and Eq. (6) is transformed into the following:

$$I_h(x_o, y_o; x_s, y_s, z_s) = \sum_{n=\frac{1-N}{2}}^{\frac{N-1}{2}} \sum_{m=\frac{1-M}{2}}^{\frac{M-1}{2}} \left| C_1(\bar{r}_s) L\left[\frac{-\bar{r}_s}{z_s}\right] \left(C_2 Q\left[\frac{f_1 - z_s}{f_1 z_s}\right] + C_3 Q\left[\frac{f_2 - z_s}{f_2 z_s}\right] \right) \cdot \text{rect}\left(\frac{x - A_x \cdot m}{A_x}, \frac{y - A_y \cdot n}{A_y}\right) * Q\left[\frac{1}{z_h}\right] \right|^2. \quad (7)$$

If A_x and A_y are wide enough and z_h is short enough then one can assume that the width of each diffraction pattern on the camera plane from each (m, n) -th aperture is approximately A_x

$\times A_y$. This assumption enables us, firstly, to perform the free space propagation from each (m, n) -th aperture along z_h , to calculate the intensity on the camera plane and, secondly, to multiply this intensity pattern by the rectangle window function. After doing that, Eq. (7) becomes as given by:

$$I_h(x_o, y_o; x_s, y_s, z_s) = \left| C_1(\bar{r}_s) L \left[\frac{-\bar{r}_s}{z_s} \right] \left(C_2 Q \left[\frac{f_1 - z_s}{f_1 z_s} \right] + C_3 Q \left[\frac{f_2 - z_s}{f_2 z_s} \right] \right) \right. \\ \left. * Q \left[\frac{1}{z_h} \right] \right|^2 \cdot \sum_{n=\frac{1-N}{2}}^{\frac{N-1}{2}} \sum_{m=\frac{1-M}{2}}^{\frac{M-1}{2}} \text{rect} \left(\frac{x_o - A_x \cdot m}{A_x}, \frac{y_o - A_y \cdot n}{A_y} \right). \quad (8)$$

Next we calculate the free-space propagation, along z_h , of the two inclined spherical waves emerging from the SLM. As has been stated previously, a point source at \bar{r}_s induces an inclined spherical wave (on some plane a distance z_s from the source) in the form of $C(\bar{r}_s) Q[1/z_s] L[-\bar{r}_s/z_s]$. Therefore, any further propagation, say along z_h , results in a complex amplitude of $C'(\bar{r}_s) Q[1/(z_s + z_h)] L[-\bar{r}_s/(z_s + z_h)]$. We conclude that if the wave distribution at some z_s plane is $C(\bar{r}_s) Q[1/z_s] L[\bar{A}]$, then at some further plane, at distance z_h far from the plane z_s , the complex amplitude can be expressed as follows:

$$u(x, y; z_h) = \left(C(\bar{r}_s) Q \left[\frac{1}{z_s} \right] L[\bar{A}] \right) * Q \left[\frac{1}{z_h} \right] = C'(\bar{r}_s) Q \left[\frac{1}{z_s + z_h} \right] L \left[\frac{\bar{A} z}{z_s + z_h} \right]. \quad (9)$$

Applying the rule of spherical wave propagations formulated in Eq. (9) into Eq. (8) yields the following intensity:

$$I_h(x_o, y_o; x_s, y_s, z_s) = \left| C'(\bar{r}_s) L \left[\frac{-f_1 \bar{r}_s}{z_h + \frac{f_1 z_s}{f_1 - z_s}} \right] \cdot Q \left[\frac{1}{z_h + \frac{f_1 z_s}{f_1 - z_s}} \right] \right. \\ \left. + C''(\bar{r}_s) L \left[\frac{-f_2 \bar{r}_s}{z_h + \frac{f_2 z_s}{f_2 - z_s}} \right] \cdot Q \left[\frac{1}{z_h + \frac{f_2 z_s}{f_2 - z_s}} \right] \right|^2 \\ \times \sum_{n=\frac{1-N}{2}}^{\frac{N-1}{2}} \sum_{m=\frac{1-M}{2}}^{\frac{M-1}{2}} \text{rect} \left(\frac{x_o - A_x \cdot m}{A_x}, \frac{y_o - A_y \cdot n}{A_y} \right) \\ = \left| C'(\bar{r}_s) L \left[\frac{-f_1 \bar{r}_s}{z_h f_1 - z_s z_h + f_1 z_s} \right] Q \left[\frac{f_1 - z_s}{z_h f_1 - z_s z_h + f_1 z_s} \right] \right. \\ \left. + C''(\bar{r}_s) L \left[\frac{-f_2 \bar{r}_s}{z_h f_2 - z_s z_h + f_2 z_s} \right] Q \left[\frac{f_2 - z_s}{z_h f_2 - z_s z_h + f_2 z_s} \right] \right|^2 \\ \times \sum_{n=\frac{1-N}{2}}^{\frac{N-1}{2}} \sum_{m=\frac{1-M}{2}}^{\frac{M-1}{2}} \text{rect} \left(\frac{x_o - A_x \cdot m}{A_x}, \frac{y_o - A_y \cdot n}{A_y} \right) \quad (10)$$

Calculating the magnitude squared expression of the first part of Eq. (10) leads directly to the final expression given in Eq. (2).